SUPPLEMENTARY INFORMATION

Grayscale-to-color: Scalable fabrication of bespoke multispectral filter arrays

---

Supplementary Information contains 29 pages.

Supplementary Notes

1. Simulations

1.1. Effect of insulator (resist) thickness on transmission
1.2. Addition of an encapsulation layer
1.3. Angle dependency

2. Fabrication

2.1. Dose variation
2.2. Proximity effect
2.3. Resist thermal reflow
2.4. Variability in optical performance across array
2.5. Pixel resolution dose tests
2.6. Materials considerations for CMOS processing

Supplementary Figures 1-24

References

Supplementary Notes

1. Simulations

1.1 Effect of insulator (resist) thickness on transmission

Supplementary Figure 1 presents simulation results (Lumerical FDTD solutions[1]) of the optical transmission through a metal-insulator-metal (MIM) stack. Due to its simplicity and customizability, the FDTD method used here is chosen as opposed to a more analytical transfer matrix / rigorous coupled wave analysis (RCWA) method.[2] The simulations are used to confirm: the origin of the resonant modes; resist (insulator) thickness required to achieve operation in the visible, and; how different parameters (e.g. layer thicknesses) affect the transmission characteristics. Hence we use the simulations to determine the required layer thicknesses of the multispectral filter arrays (MSFAs). The simulations for the MIM stacks (in *Supplementary Figure* S1**:** *main manuscript*) were performed using periodic boundary conditions parallel to the propagation direction of the incident electromagnetic wave and perfectly matched layers tangential to the incident wave. Plane waves (300—1000 nm spectrum) are injected toward the structure from the SiO_2 side and a power monitor several microns away from the structure is used to calculate the transmission. The resist (insulator) layer is assigned a real-only refractive index value (n = 1.635), obtained through the MaN-2400 series photoresist datasheet [*Micro resist technology GmbH*]. The other layers are assigned a complex and dispersive refractive index from Lumerical FDTD solutions: Ag model - Johnson & Christy; SiO_2 – Palik; MgF_2 – model fitted to tabulated values. Ag is chosen as the mirror material due to considerations of its complex dielectric function in the visible and near-infrared part of the spectrum.[3–6] Based on **Supplementary Figure 1** the simulations indicate that as the insulator layer increases the Fabry-Perot-type mode red-shifts accordingly (due to an optical path length increase) and the mirror thicknesses (c) control the Q-factor of the cavity (linewidth). As a result, a metal thickness of ~25—30 nm results in a suitable tradeoff between transmission and FWHM.

1.2 Addition of an encapsulation layer

Depositing an inert capping layer on top of the MIM stack provides chemical and mechanical durability, preventing oxidation and increasing rigidity. A material such as MgF_2 (similar to quartz) provides these qualities. It is relatively inert, mechanically rigid, optically transparent and moreover, relatively straightforward to deposit post-metallization of the second mirror. **Supplementary Figure 2** shows the simulation of the transmission of the Ag (26 nm)-MIM stack (125 nm insulator) as a function of MgF_2 encapsulation layer thickness (0—50 nm). A dispersive material model[7] is used for its refractive index. It is observed the transmission peak slightly shifts to longer wavelengths with increasing MgF_2 thickness and increases a small amount. The FWHM also gradually increases. We therefore conclude that the encapsulation layer provides negligible degradation in transmission characteristics, and if anything, slightly improves them.

1.3 Angle dependency

In imaging optics, a high *F*-number (numerical aperture ~ 0) typically implies parallel rays incident on the sensor array, while a low *F*-number implies the rays arrive at an angle (numerical aperture > 0). For multi-layered MSFAs, the spectral response is often a function of incidence angle, which in combination with polarization angle, affects the transmission characteristics of the filter.

Supplementary Figure 8 shows FDTD simulations (Bloch boundary conditions and angled source using BFAST conditions) of the MIM structure under orthogonal incident polarizations (TE and TM) for varying angles of incidence up to 60º. For conventional CMOS image sensors, the chief ray angle (CRA) – broadly defining the cone of angles incident upon the center top of the pixel – can be up to ± 30° (with the larger angles, e.g. 30°, more commonplace in smartphone sensors). It can be observed that, between 0 — 30º incident angle, the peak spectral position varies from ~590—578 nm (Δλ ~ 12 nm) for TM and from ~590 — 565 nm (Δλ ~ 25 nm) for TE. The transmission intensity remains relatively constant (~85%) across these angles. The FWHM (~36 nm at 0º, for TM and TE) narrows slightly by ~5 nm for TE, and for TM widens by ~15 nm (at 30º). Beyond 30º, the spectral shift increases more significantly, especially for TE-polarization.

For interference filters in general, there is typically a blue-shift of the resonant peak arising from a phase-shift reduction in the dielectric layer for larger angles.[8] For interference based optical filters, there are methods to compensate for such a spectral shift, including: in-plane nanostructuring; incorporation of additional dielectric layers; and addition of microlens arrays.[8,9] Conversely, for the relatively thin (<200 nm thick) Ag-MIM filters here, that only support first-order FP-type modes, the angular dependency is somewhat reduced compared to thicker structures with a high number of alternating index layers. The small vertical-to-lateral aspect ratio of the MIM pixels result in relatively small angle dependency.

2. Fabrication

2.1 Dose variation

As described in the main manuscript, the effect of exposure dose and correct choice of development time (and developer) controls the final thickness of the remaining resist (insulator) in a MIM cavity, hence controlling the center position of the transmission spectra. To demonstrate this, **Supplementary Figure 3** shows the transmission spectra of a set of 5 μm pixels which vary in exposure dose across three different development times. It can be observed—both quantitatively in (a) and visually in (b)—that for a constant dose range (0.1–0.7 Cm^{-2} here) the position of the peak blue-shifts with increasing development time. As the developer is selectively removing resist that has not been sufficiently cross-linked (due to MaN-series photoresist being negative tone), a longer development time results in more resist being removed, hence thinner cavity and shorter wavelength mode. This is further illustrated in **Supplementary Figure 5**, which shows a rectangular array with transmission wavelength across the visible spectrum and respective SEM micrograph.

Supplementary Figure 5 shows a custom dose/resolution pattern fabricated 4 times (i—iv) across a sample, with the dose incremented by +0.125 Cm^{-2} each time. The pattern itself consists of 100 separate layers; each layer corresponds to a linearly increasing dose within the range 0.1–0.4 Cm^{-2}. The figure, and in particular the magnified regions in (b) and (c), visually shows the main operating principle of this work: exposure dose controls the wavelength of transmission.

2.2 Proximity effect

In EBL, the proximity effect is the unwanted exposure of regions adjacent to the pattern being exposed due to electron scattering events in the resist. The proximity effect can be lessened through the translation of the grayscale MSFA approach to larger batch processing i.e. photolithography. However, for this work (in which EBL is utilized) as the density of features increases, the proximity effect is more pronounced. In this work, each filter pixel has its center wavelength defined by a specific exposure dose. As a result of the proximity effect, the total dose applied to a specific region (pixel) is additionally dependent on the dose applied to surrounding pixels.[10,11]

The proximity effect can be observed by comparing the patterning of isolated pixels (i.e. arrays with non-exposed spacing between pixels) to dense arrays; the dose required to achieve a specific wavelength (resist thickness) is lower in dense arrays than it is in isolated regions. **Supplementary Figure 6** (a) shows an optical micrograph (transmission) of the dose test array, in which the regions (1) and (2) are arrays of equally sized pixels which both also equally increase in exposure dose (from ~0.17—0.52 Cm^{-2}; 10s development time), but with ‘isolated’ and ‘dense’ configurations respectively. It is observed that the arrays in (2) are highly red shifted in transmission indicating a larger thickness in remaining resist and thus greater accumulated exposure dose. This is due to the unwanted cumulative adjacent exposure from the neighboring pixels. **Supplementary Figure 6** (b) is an additional example of the effect: a 1951 USAF resolution target, in which each element of the line triplets is given a different exposure dose. The final thickness/filtered wavelength is a function of spatial position within the rectangle as the averaged dose density is larger at the center of the rectangle than it is in the corner/edges.

The impact of the proximity effect in a Bayer filter array was investigated by examining the transmission characteristics of a 3-channel RGB array as a function of position from the edge of the array **(Supplementary Figure 7).** The center wavelength of the transmission peak (in both green and blue pixels) appears to remain relatively constant following a sharp change approximately 50–100 μm from the edges. This is likely due to the cumulative dose density remaining approximately constant for pixels away from the edge of the array, a consequence of the periodic array pattern. A simple empirical correction adopted for this work was to 'over pattern' each MSFA, such that the area of interest (image sensor area) is >100 μm from the edge of the MSFA pattern. This approach also demands reducing the dose profile to compensate for increased cumulative exposure in the central region. It would also be possible to perform Monte Carlo electron scattering simulations for each pattern to optimize the dose patterns and avoid this empirical correction, however, the commercial software to perform these simulations was not available for this study.

2.3 Resist thermal reflow

Thermal reflow is a fabrication processing technique that involves the thermal treatment of a photoresist (post-development) such that the resist is brought to a temperature ≳ glass transition temperature.[12] By doing so, the resist 'reflows', fully or partially depending on the temperature and time, which can be used to smooth the resist. The technique, for example, can be used to turn staircase-like 3D-pattens to 3D slopes,[12] or to fabricate microlens arrays. In this work, shown with several examples in **Supplementary Figure 21**, we used thermal reflow to smooth the resist surface post-development, but pre-second metal mirror deposition, to flatten/smooth the second mirror surface, narrowing the FWHM and boosting transmission efficiency.

2.4 Variability in optical performance across array

The intra- and inter-chip variability of the optical characteristics of fabricated MSFAs is shown in **Supplementary Figure 10** and **Supplementary Figure 11**. For each MSFA, a range of unit cells were chosen at random across the array (but at least 100μm from the border of the array due to the proximity effect issue described in Section 2.2) and the filter spectra were recorded and analyzed using an optical microscope. **Supplementary Figure 10** shows the variability in peak wavelength across different pixels for RGB MSFAs (i.e. Bayer mosaics) for three different processing recipes corresponding to three differently processed separate chips (listed below, *Recipes 1—3*). (a) and (b) are of two different dose (*D*) profiles for the 3-channels. For each 'recipe' (described in the caption), spectra of four randomly positioned unit cells were analyzed (4x 3-channels = 12 points) i.e. 4 transmission spectra per channel (wavelength band).

Supplementary Figure 11 shows box plots of the optical transmission characteristics of a range of MSFA geometries fabricated across three different chips (i.e. the three different recipes from **Supplementary Figure 10**). These include 2 x 3-channel designs (RGB1 and RGB2), RGB+1, and 3x different 3x3 mosaics (each with a varying dose profile range). The three different recipes correspond to the following processing conditions:

Recipe 1 = pre-development thermal treatment (90ºC, 60s) + normal processing*;
Recipe 2 = normal processing*;
Recipe 3 = normal processing* + post-development thermal treatment (100ºC, 30s).
* *normal processing recipe described in Methods - main manuscript.*

It can be observed from both figures that the variation in optical performance characteristics is minimal within each respective array. For example, the respective channel peak wavelength shift

is typically ≲5nm across the arrays and different recipes (**Supplementary Figure 11b)**. Moreover, it can be concluded from these results that the addition of baking steps to the standard protocol enhances the peak transmission. As shown in **Supplementary Figure 11 (a)** adding a post-development bake (Recipe 3) increases the peak-transmission up to ~80%. The FWHM is also improved (**Supplementary Figure 11c**) through adding additional thermal treatment; decreasing to ~50 nm in comparison to the standard protocol.

2.5 Pixel resolution dose tests

In the main manuscript, we use 11µm x 11µm pixel dimensions, primarily due to limitations with the experimental image sensor setup, however, these length scales can be easily reduced. To demonstrate such scalabilty, we fabricated arrays where exposure dose is varied linearly, with pixel sizes range from: 5.5 µm down to 460 nm (**Supplementary Figure 12**) Note, 460 nm is not the upmost limit to resolution but for this pixel dimension, the range of lateral-to-vertical aspect ratios of ~9:1 (e.g. ~450 nm:50 nm) to ~9:4 (e.g. ~ 450 nm:200 nm) meaning that they exhibit low aspect ratios and are mechanically stable, hence we suspect the resolution can extend beyond what is demonstrated here. In addition, **Supplementary Figure 13** shows a series of angled SEM micrographs of 1 µm and 500 nm pixels showing the surface morphology, and their uniformity at these size scales.

2.6 Materials considerations for CMOS processing

Even though SU-8 is a thermally and chemically stable photoresist, a longer-term solution would be to use glass (SiO_2), which could be achieved using the grayscale resist as an etching mask for a reactive ion etching step (see **Supplementary Figure 22**). The use of thin-film Ag similarly provides a potential challenge in the form of long term chemical stability. By encapsulating Ag with chemically inert and optically transparent thin films, such as silicon oxide, this issue is lessened. However, a more comprehensive approach would be to replace the Ag with alternating high-low index all-dielectric mirrors operating with a cut-off wavelength of ~400 nm, thus passing the visible-NIR. These mirrors typically require a minimum of 3 thin-film layers[13] and can be deposited easily within a reactive sputtering or e-beam evaporation step (akin to the metallic mirrors here).

Figures

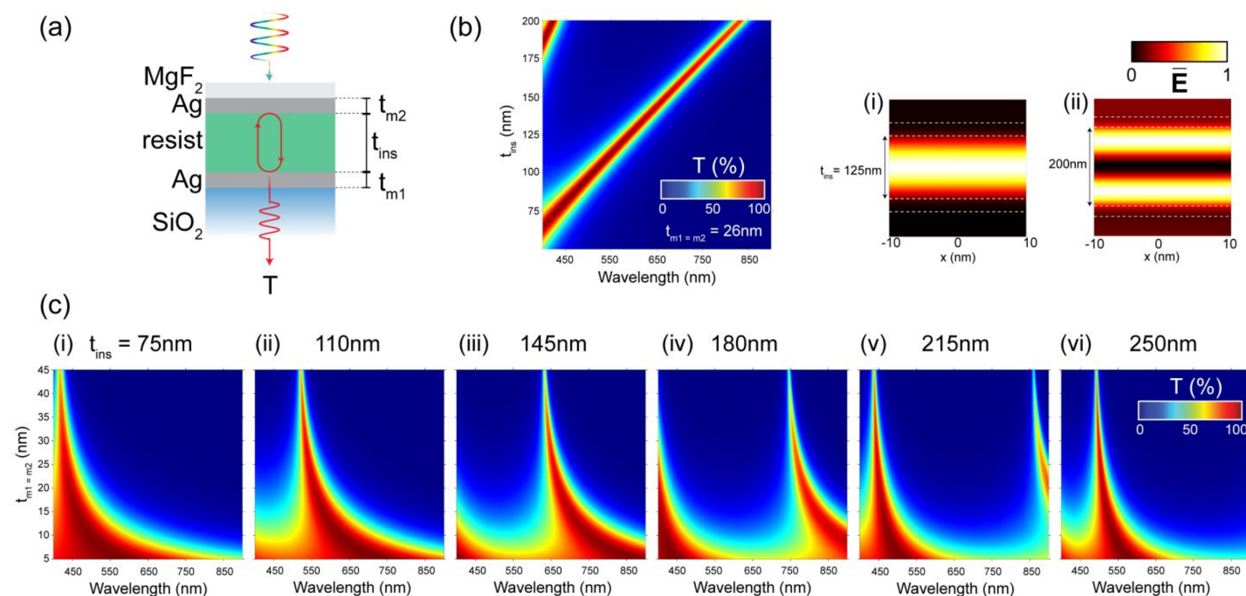

Supplementary Figure S1. FDTD simulation of the optical transmission from a Ag-MIM stack. (a) Schematic of MIM geometry used in simulation. (b) FDTD simulation of the transmission from the Ag-MIM-MgF_2 (encapsulation) stack as a function of insulator (resist) thickness. (i) normalized electric field intensity map for insulator thicknesses of 125 nm (at λ = 580 nm) and (ii) 200 nm (at λ = 580 nm) corresponding to first-order and second-order resonances respectively. (c) shows the effect of metal mirror (Ag) thickness on the transmission spectra for varying insulator thicknesses (75 – 250 nm).

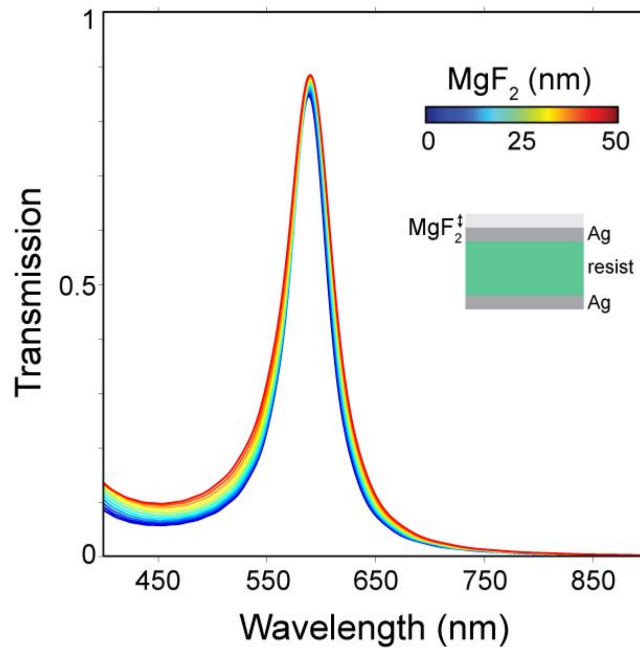

Supplementary Figure S2. Effect of the addition of a MgF_2 encapsulation layer. FDTD simulation of the transmission through the Ag-MIM stack in **Figure 1**, but with the addition of an encapsulation layer with varying thicknesses, from 0—50 nm.

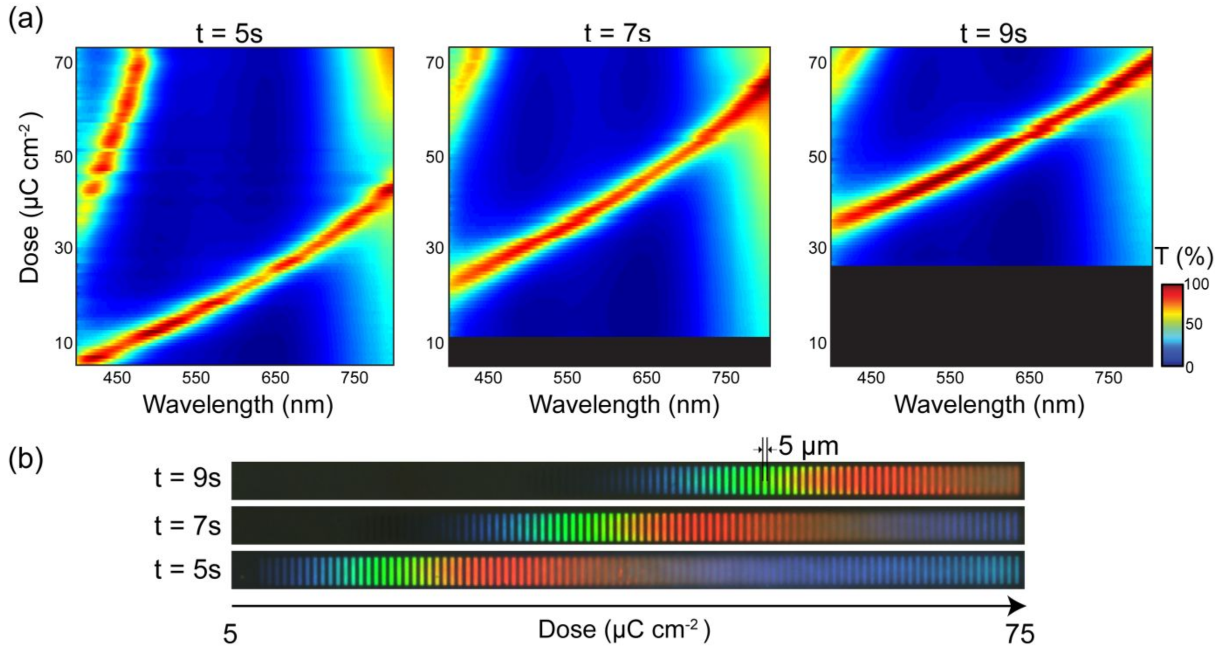

Supplementary Figure S3. The effect of dose variation and development time. (a) Measured transmission spectra, as a function of exposure dose (μC cm^{-2}), for three different development times. (b) optical micrographs of a set of 5 μm wide rectangles with varying exposure dose for three development times. MaN-2405 resist is used along with full concentration AZ 726 MIF developer; as described in the *Methods*.

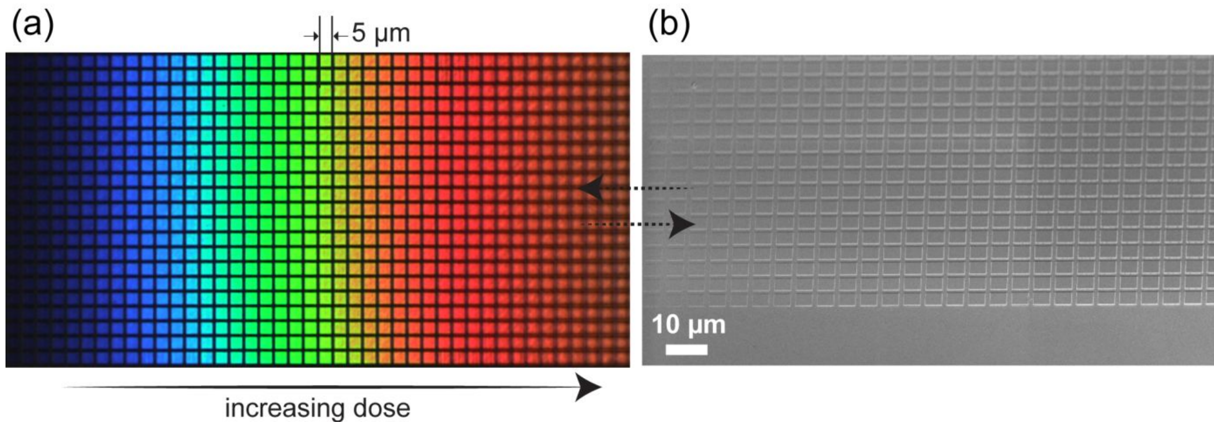

Supplementary Figure S4. Increasing exposure dose with 5 μm pixels. (a) Optical micrograph (transmission) of an array of 5 x 5 μm squares (pixels) which linearly increase in exposure dose (left-to-right). The increase in dose results in a thicker remaining resist (insulator in MIM cavity) hence red-shifted transmission characteristics. (b) An SEM micrograph of the same area in (a) in which the variation in height (from left-to-right) can be observed.

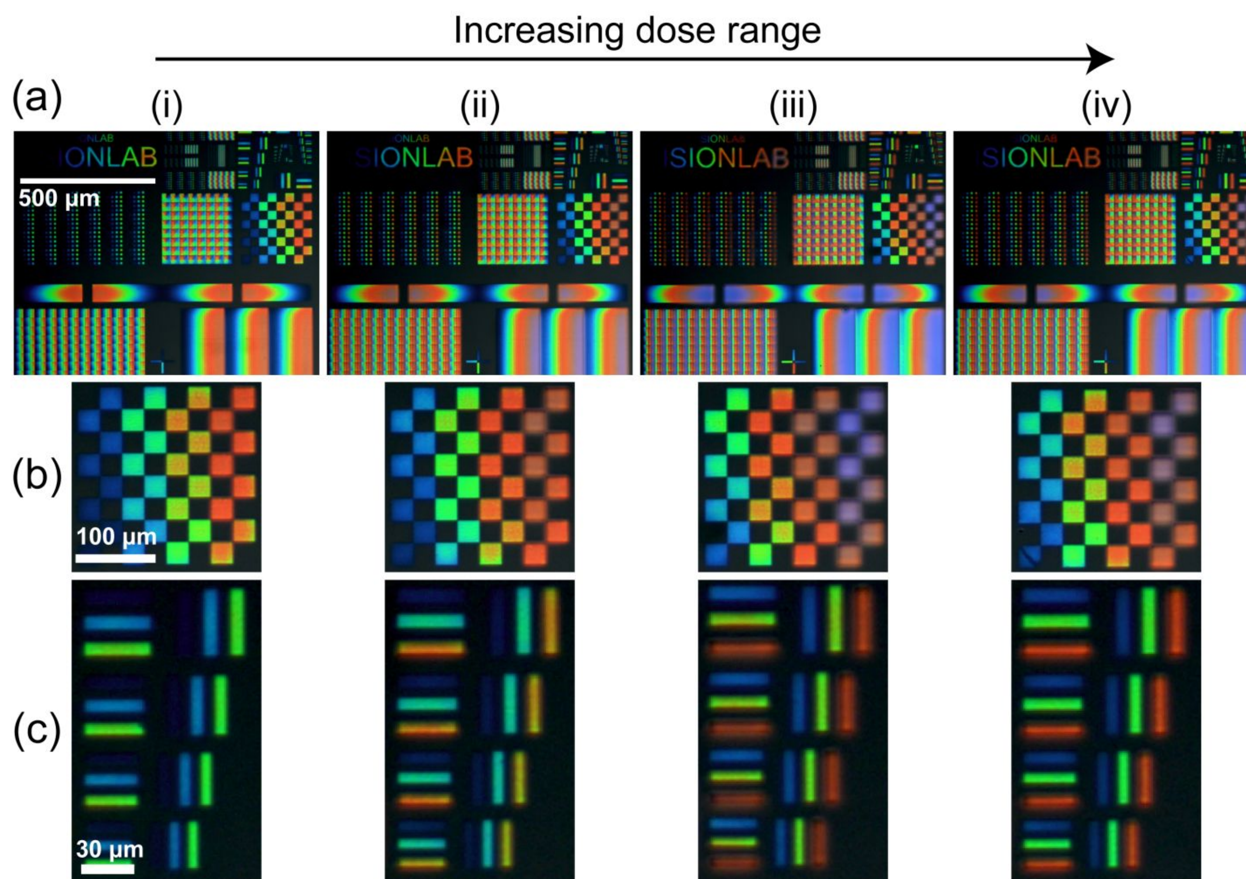

Supplementary Figure S5. Dose/Resolution test with increasing dose limits. (a) A custom resolution pattern in transmission under the optical microscope, composed of 100 different layers in which each layer has a distinct exposure dose between the (linear) range (i) 0.1–0.4 Cm^{-2}, with (ii – iv) increasing by +0.125 Cm^{-2} each time. The sample is processed as described in the Methods. (b) and (c) show digitally zoomed in regions of specific areas of the dose/resolution test in (a). In (c), there are three different doses (one for each lined element), starting in (i): 0.16, 0.25, 0.34 Cm^{-2}. The figure effectively shows the change in spectral position of the FP-like mode of the MIM filter with varying exposure dose.

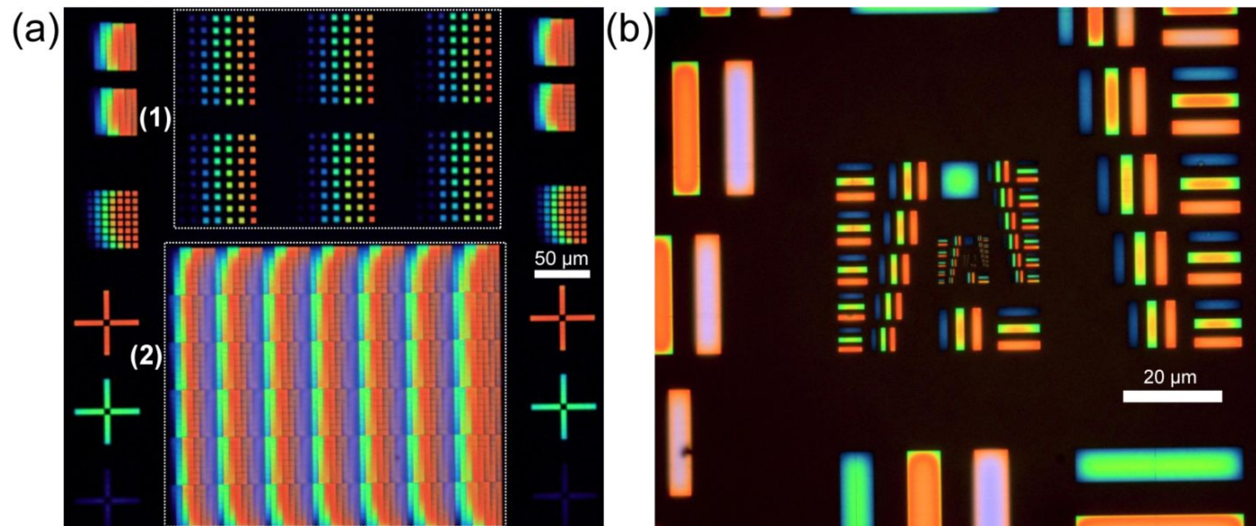

Supplementary Figure S6. Visual example of the proximity effect using resolution test grids. (a) Dose test array in which the square pixels – shown in (1) and (2) – are the same size but vary in spacing. In (2) the proximity effect causes the final pixel thickness to be greater than in (1) due to the additional exposure from adjacent pixels. In (b), the proximity effect is highlighted in a USAF 1951 resolution target in which each element (in the line triplet) is given a different dose (hence different final wavelength). However, due to the increased 'dose density' in the center of the rectangle compared to the corners/edges, the final thickness and hence wavelength is different.

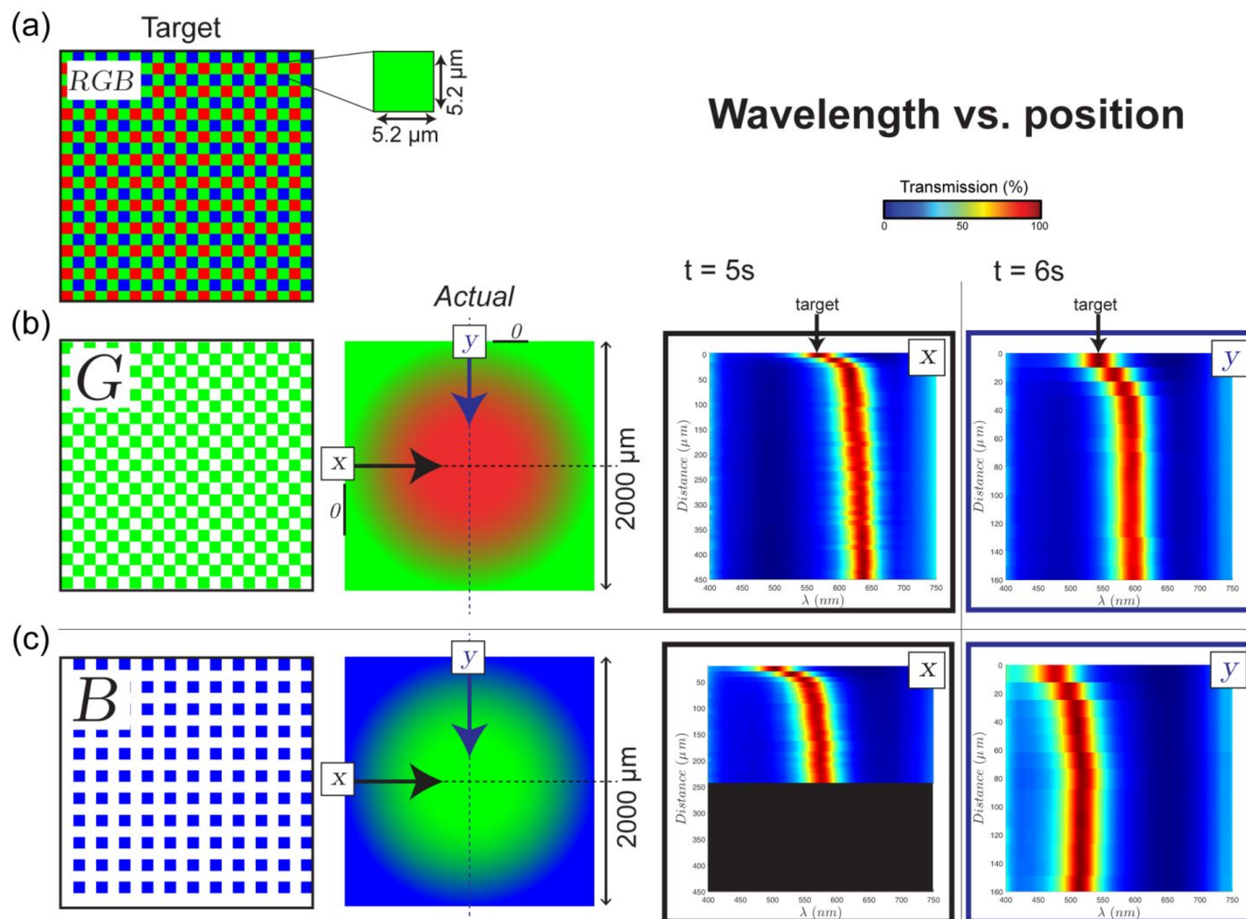

Supplementary Figure S7. Proximity effect demonstration on RGB array. (a) Desired final pattern: RGB CFA array. (b) and (c) are the desired green and blue channel mosaics respectively, with an exaggerated visual example of how the final color varies as a function of spatial position. Experimentally measured optical transmission of the respective wavelength channels in an RGB array as a function of distance from the edge of the patterned array, for two different development times.

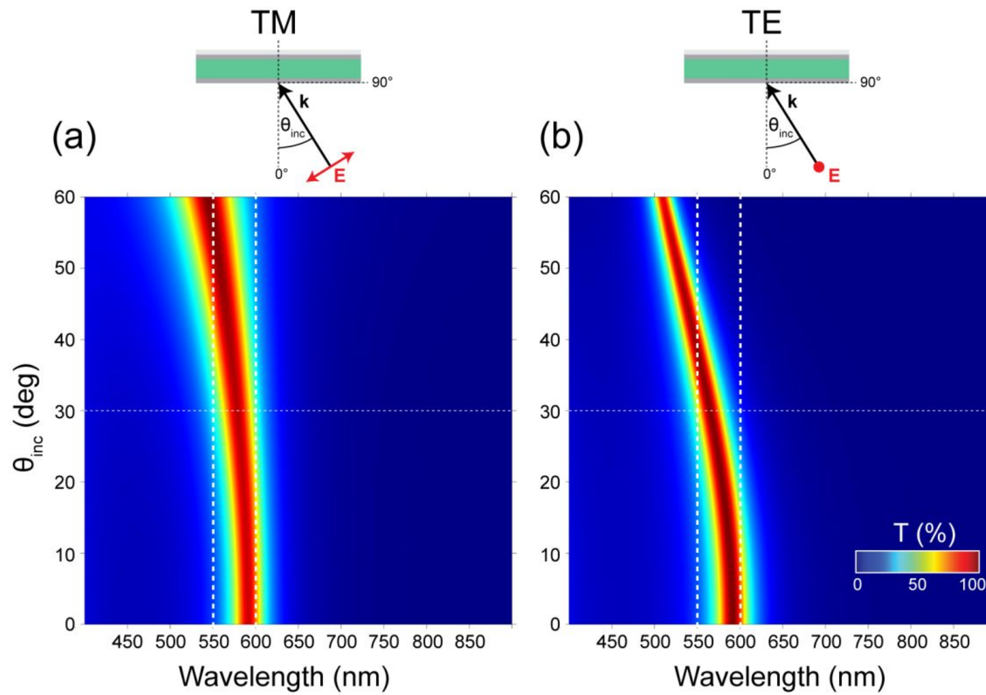

Supplementary Figure S8. MIM stack transmission spectra. (a) TM-polarized input wave, and (b) TE-polarized input wave, for various angles of incidence, from 0—45 degrees from normal. The composition of the MIM layers is described in the main manuscript.

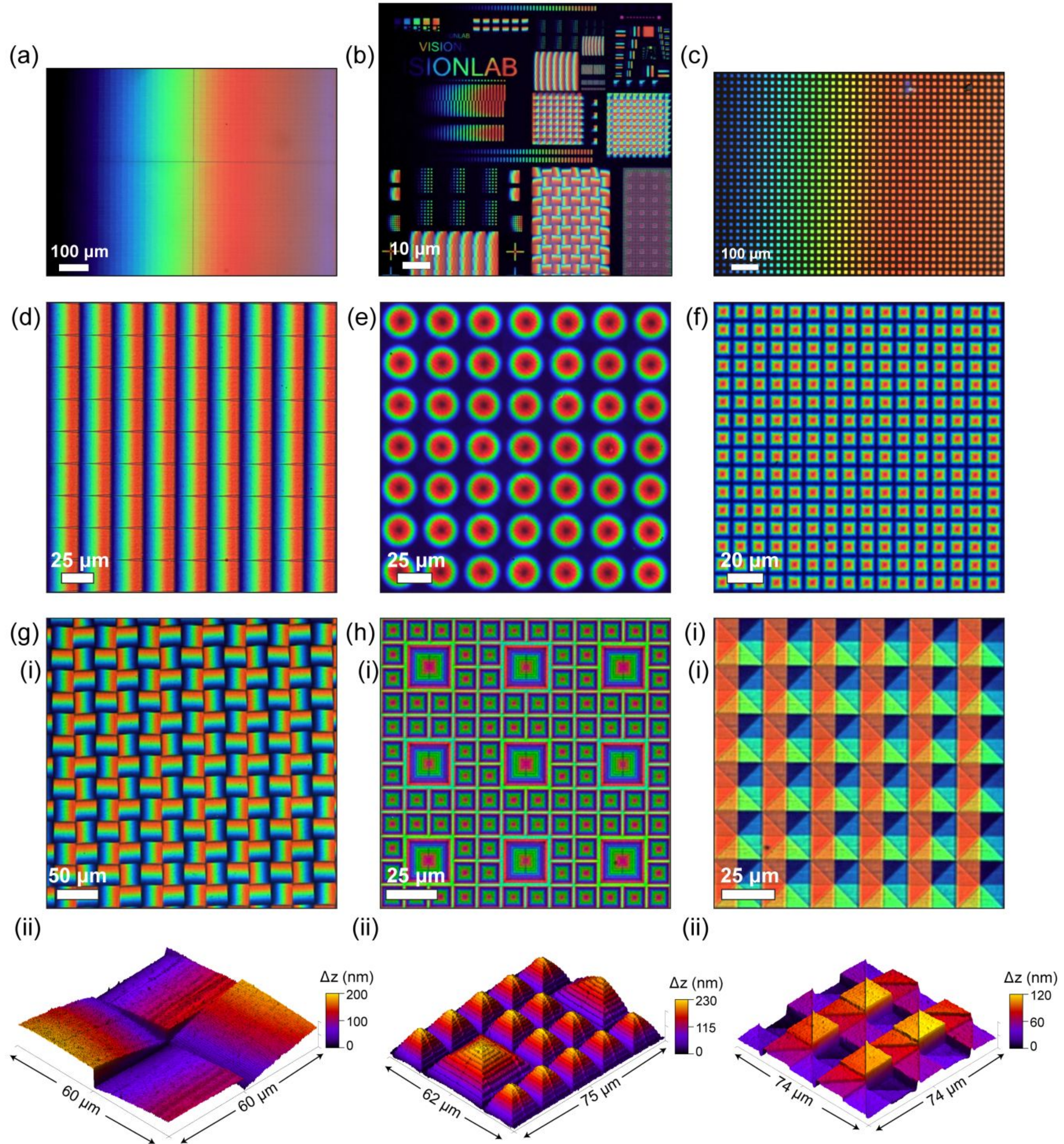

Supplementary Figure S9. A variety of designs illustrating the versatility of the approach in this work. This figure illustrates the customizability and power of the framework presented in this work, as all of the different designs chip (a—i) are fabricated with a single lithographic step on the same chip with the same materials (using the recipe in the Methods; main manuscript).

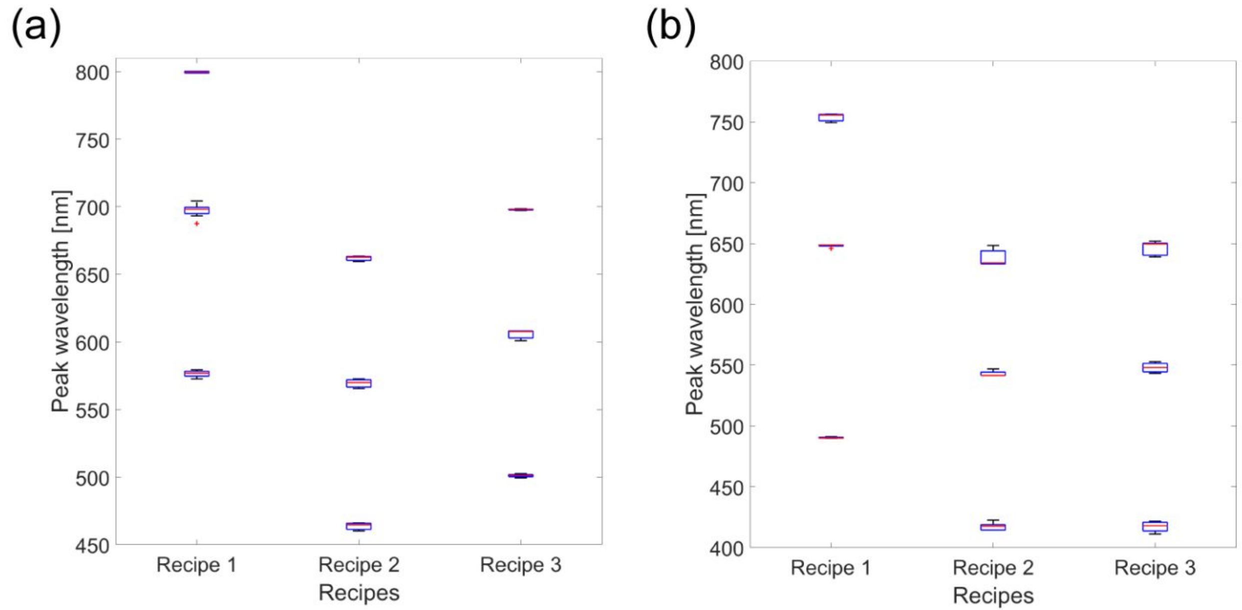

Supplementary Figure S10. Peak wavelength box plots of RGB MSFAs for three different recipes. (a) and (b) correspond to two different dose sets for red, green and blue channels: i.e. $D_{B,G,R}$ = 0.2, 0.3, 0.4 Cm^{-2} for (a), and $D_{B,G,R}$ = 0.15, 0.275, 0.375 Cm^{-2} for (b). Within each sub-figure, there are three different recipes; described previously. For each recipe, ~16 filter pixels (spectra) per channel (e.g. RGB = 3) were recorded. The red central lines correspond to the median values, and the bottom and top edges of the box indicate the 25th and 75th percentiles respectively. The whiskers extend to the most extreme data points and the outliers are plotted individually (red '+' symbol).

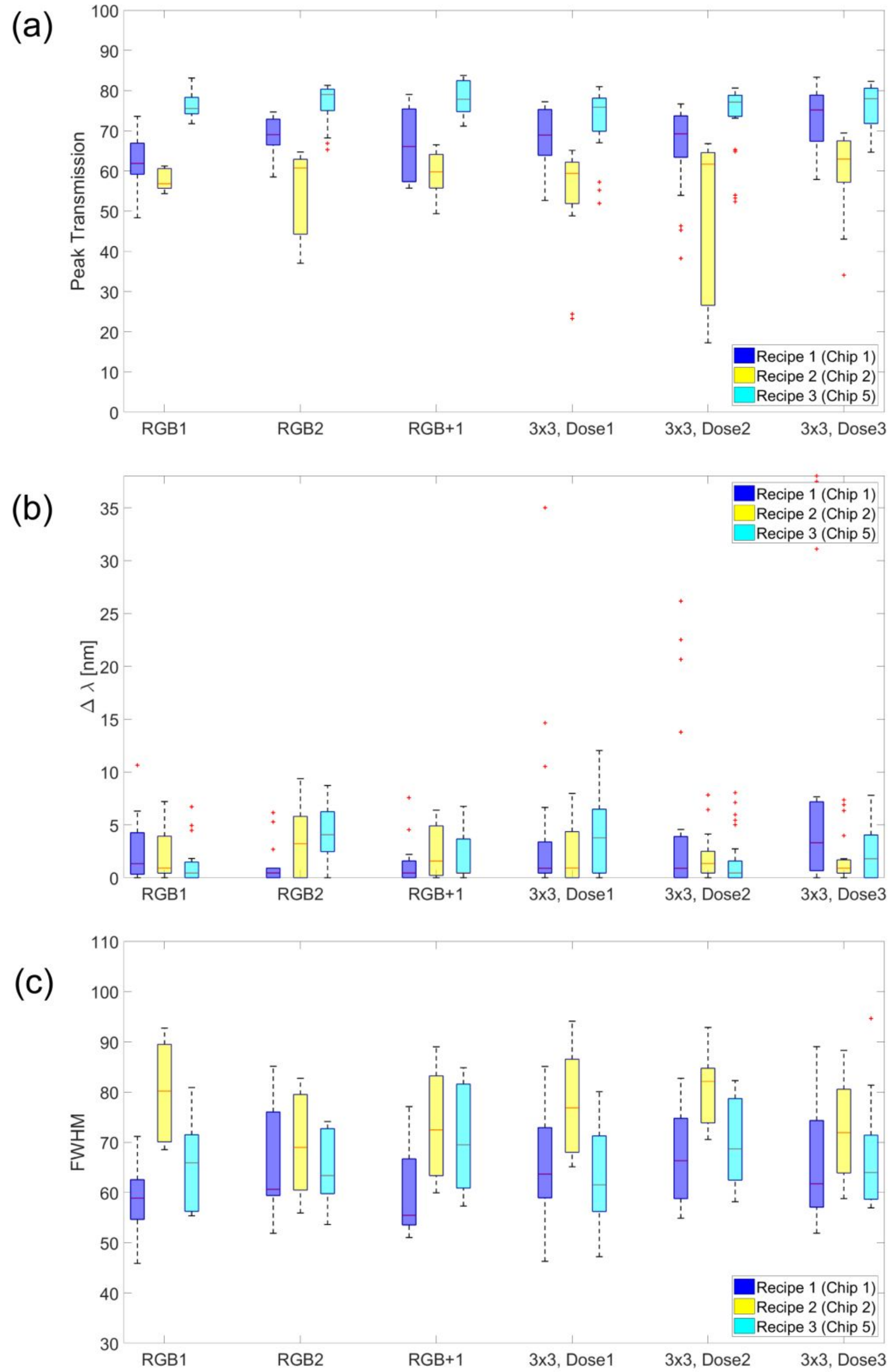

Supplementary Figure S11. Box plots of the optical characteristics from a series of MSFA patterns from three different recipes. (a) Peak transmission, (b) Peak wavelength shift, Δλ, from the average (i.e. $\Delta\lambda = |\lambda - \lambda_{av}|$) and (c) FWHM. The red central lines correspond to the median values, and the bottom and top edges of the box indicate the 25th and 75th percentiles respectively. The whiskers extend to the most extreme data points and the outliers are plotted individually (red '+' symbol). For every CFA, several unit cells in the middle of each array were picked randomly and the spectrum of each pixel was recorded. For the fewer band (<4) MSFAS, ~12 spectra were recorded for each recipe. For the larger band MSFAs, 18–27 spectra were recorded for each recipe.

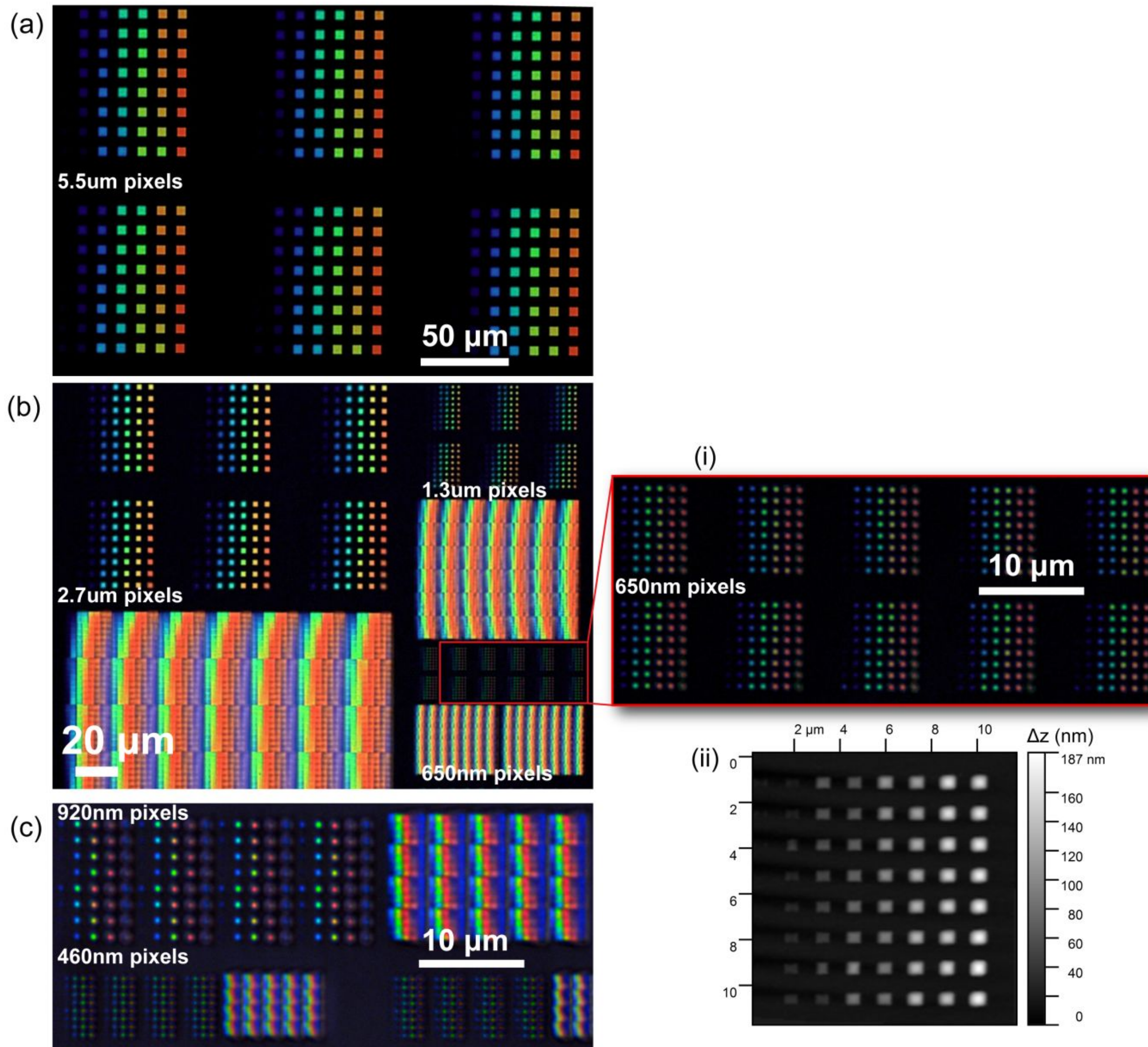

Supplementary Figure S12. Resolution of pixels in this study. A range of square pixels based on the grayscale MIM approach in this work under the optical microscope in transmission. (a) 5.5 µm lateral size pixels; (b) a range of pixel sizes from 2.7 µm, 1.3 µm and 650 nm; (i) is obtained with a higher magnification objective (100x) and (ii) is an AFM micrograph of one of the 650 nm pixel size sub-arrays in (i). (c) 920 nm and 460 nm pixel sizes. These resolution dose tests are fabricated as described in the Methods.

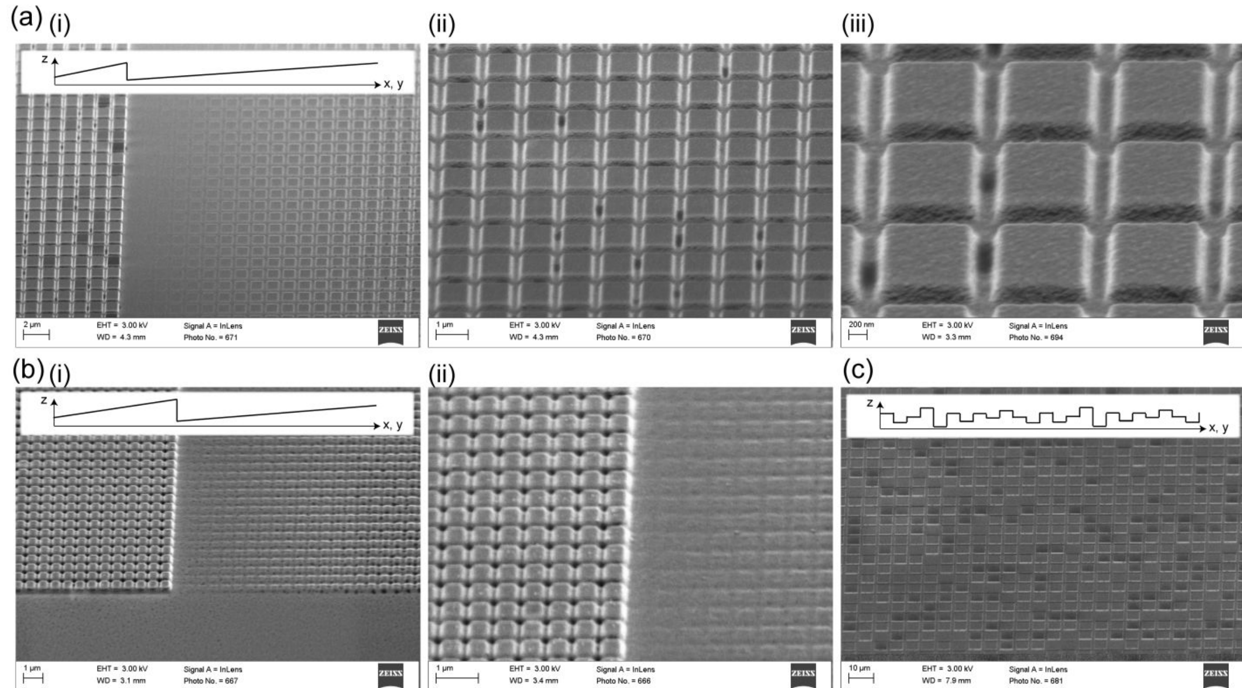

Supplementary Figure S13. SEM micrographs of MIM pixel arrays. (a) 1μm pixel array in which the dose (and thus final insulator thickness) varies in 1D. This 1D dose variation repeats (highlighted by the *inset*), with the transition shown in (i) and increasing magnifications shown in (ii) and (iii). (b) As in (a), but with a 500 nm pixel array. (c) A random dose array for 1 μm pixels.

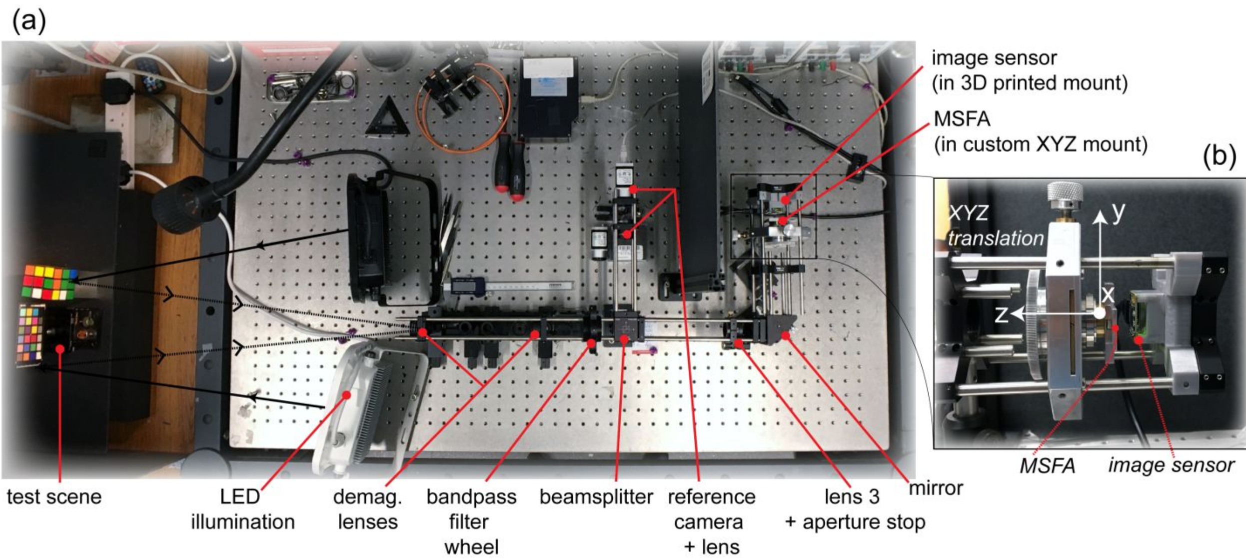

Supplementary Figure S14. **Optical imaging setup**. (a) Photograph of the optical system used for imaging experiments, in which a multispectral test scene (color chart and Rubik's cube here; left) are illuminated with 2x white light LED sources, the reflected light is de-magnified then imaged onto a monochrome image sensor through a custom MSFA. (b) shows a different viewing angle on the MSFA located in an in-house built XYZ-translation cage

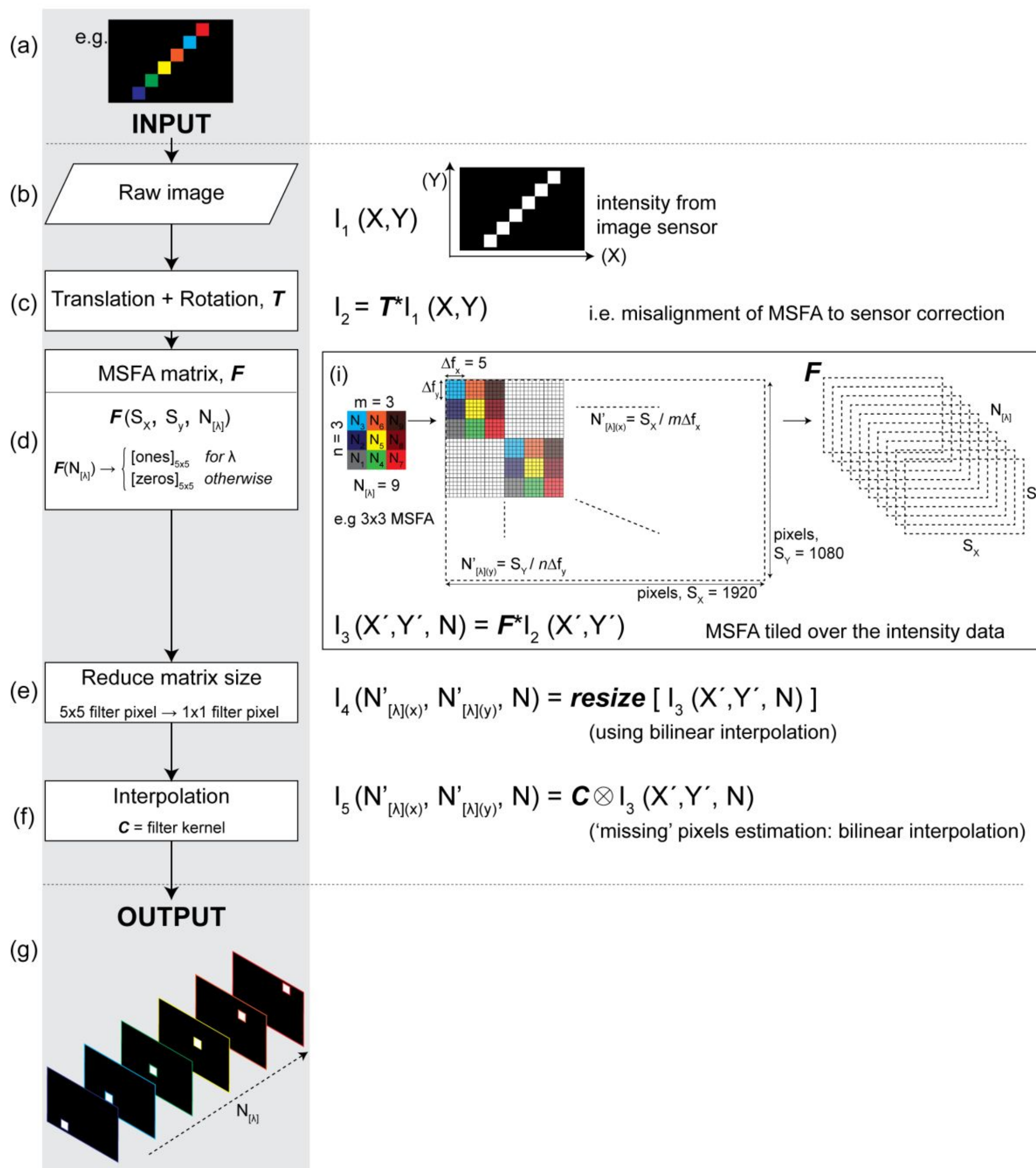

Supplementary Figure S15. Algorithm flow chart used to demosaic the images acquired through the MSFA. (a) Multispectral test scene is imaged onto the image sensor and a 2D-intensity matrix (0—255) is recorded; the raw image (b). A homogenous transformation matrix (T), incorporating a rotation by an arbitrary angle followed by a linear translation, is applied to the raw image (c), to account for the misalignment of the MSFA to the image sensor. This transformed matrix is then multiplied by a MSFA matrix (with N-bands), (d), which decomposes the 2D-intensity matrix into N x 2D matrices (one for each wavelength band). The mapping of filter pixel to image sensor is then taken into account in the MSFA matrix. This matrix is then reduced in size by a factor of 5 in each dimension (through bilinear interpolation). Finally, each channel is interpolated (d) by a pixel specific filter kernel (akin to Bayer filter demosaicing) to estimate the missing pixels between actual data. The output (g) is then N x 2D matrices: one for each wavelength band.

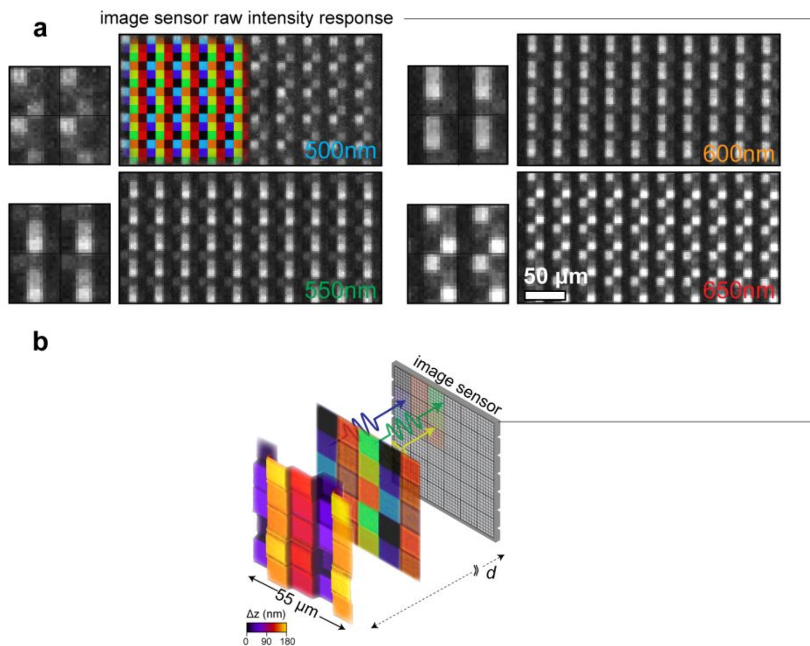

Supplementary Figure S16. **Optical imaging setup**. (a) Photograph of the optical system used for imaging experiments, in which a multispectral test scene (color chart and Rubik's cube here; left) are illuminated with 2x white light LED sources, the reflected light is de-magnified then imaged onto a monochrome image sensor through a custom MSFA. (b) shows a different viewing angle on the MSFA located in an in-house built XYZ-translation cage

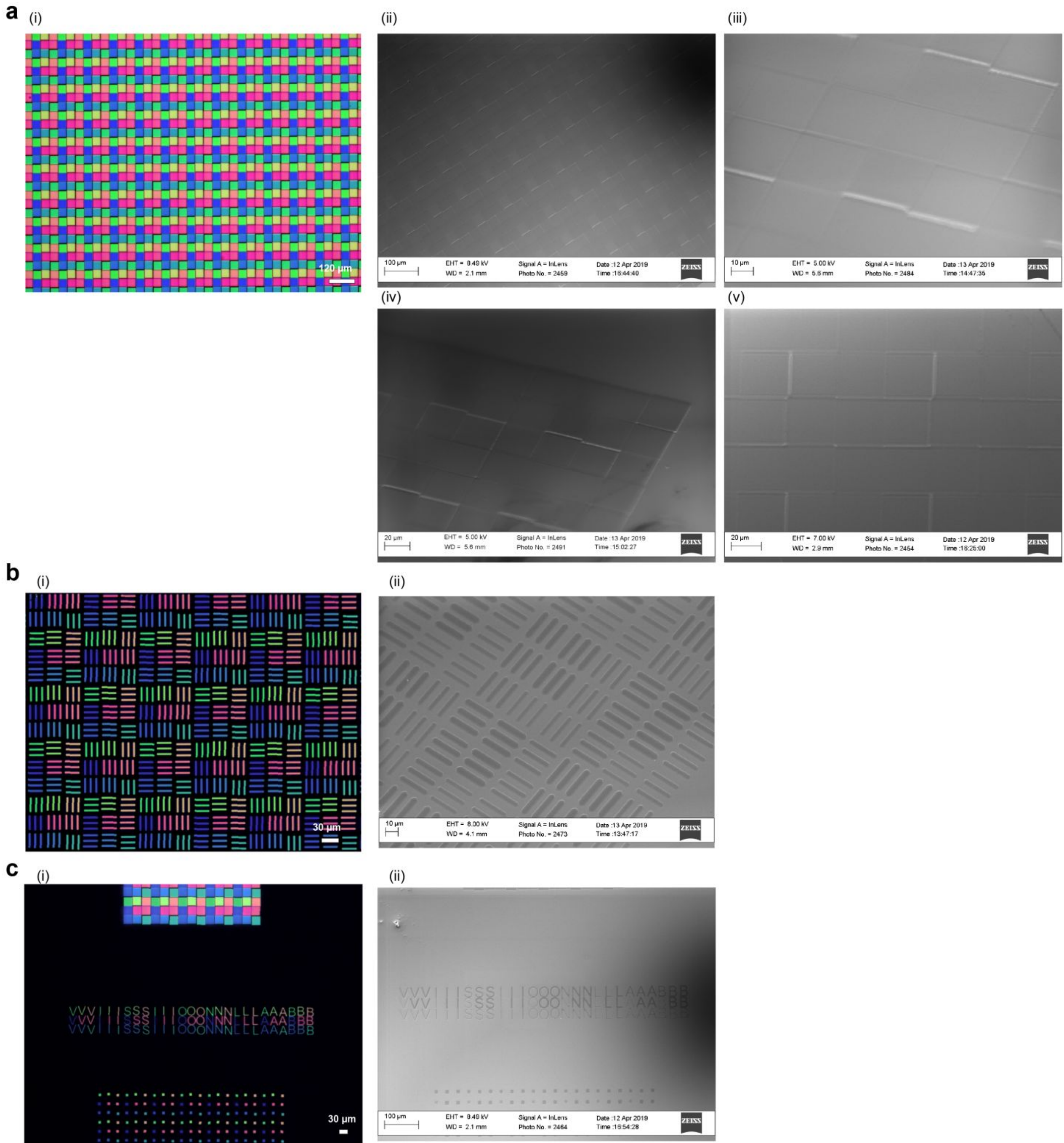

Supplementary Figure S17. Regions of the finished MSFA wafer under an optical microscope and SEM. (a) Wafer level processed MSFA, as reported in Fig.5 (main manuscript), under the optical microscope in transmission (i) and corresponding regions under different magnification under tiled SEM (ii—v). (b) Custom [x,y] alignment markers with 5 µm width and 25 µm length used to identify the degree of in-plane pixel mis-alignment; optical micrograph (i) and SEM micrograph (ii). (c) The University of Cambridge research group (*VisionLab*) text, with 5 µm character linewidth patterned onto the wafer; optical micrograph (i) and SEM micrograph (ii).

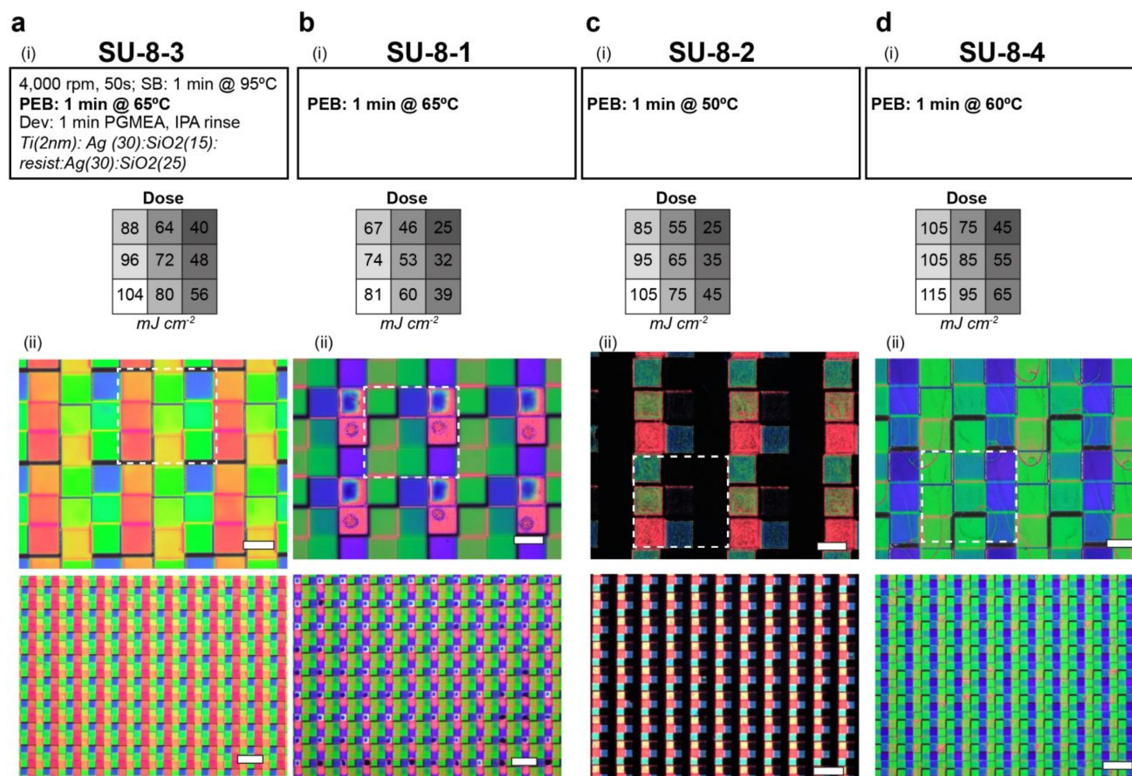

Supplementary Figure S18. Empirical optimization of different processing parameters in wafer scale fabrication of MSFAs. (a—d) Four separate wafers processed with different dose matrices and post-exposure bake (PEB) temperatures (i) which governs the degree of cross linkage. The final MSFA, under the optical microscope in transmission is shown in (ii) for the respective wafers.

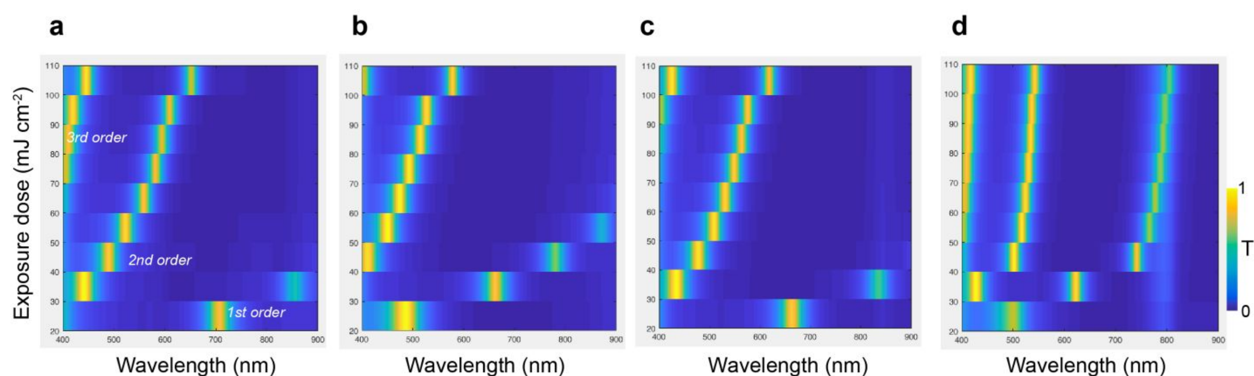

Supplementary Figure S19. Transmission spectra as a function of exposure dose in MSFA mosaic. Four separate wafers processed with similar dose matrices (represented on the y-axis) but different processing parameters: PEB 65°C for 2min: development of (a) 30s, (b) 1min, (c) 2min; and PEB 95°C for 2 min: development of (d) 1 min. PEB strongly related to final resist (insulator) due to governing degree of cross linkage. Transmission spectra obtained using optical characterization setup in Suppl. Fig 15.

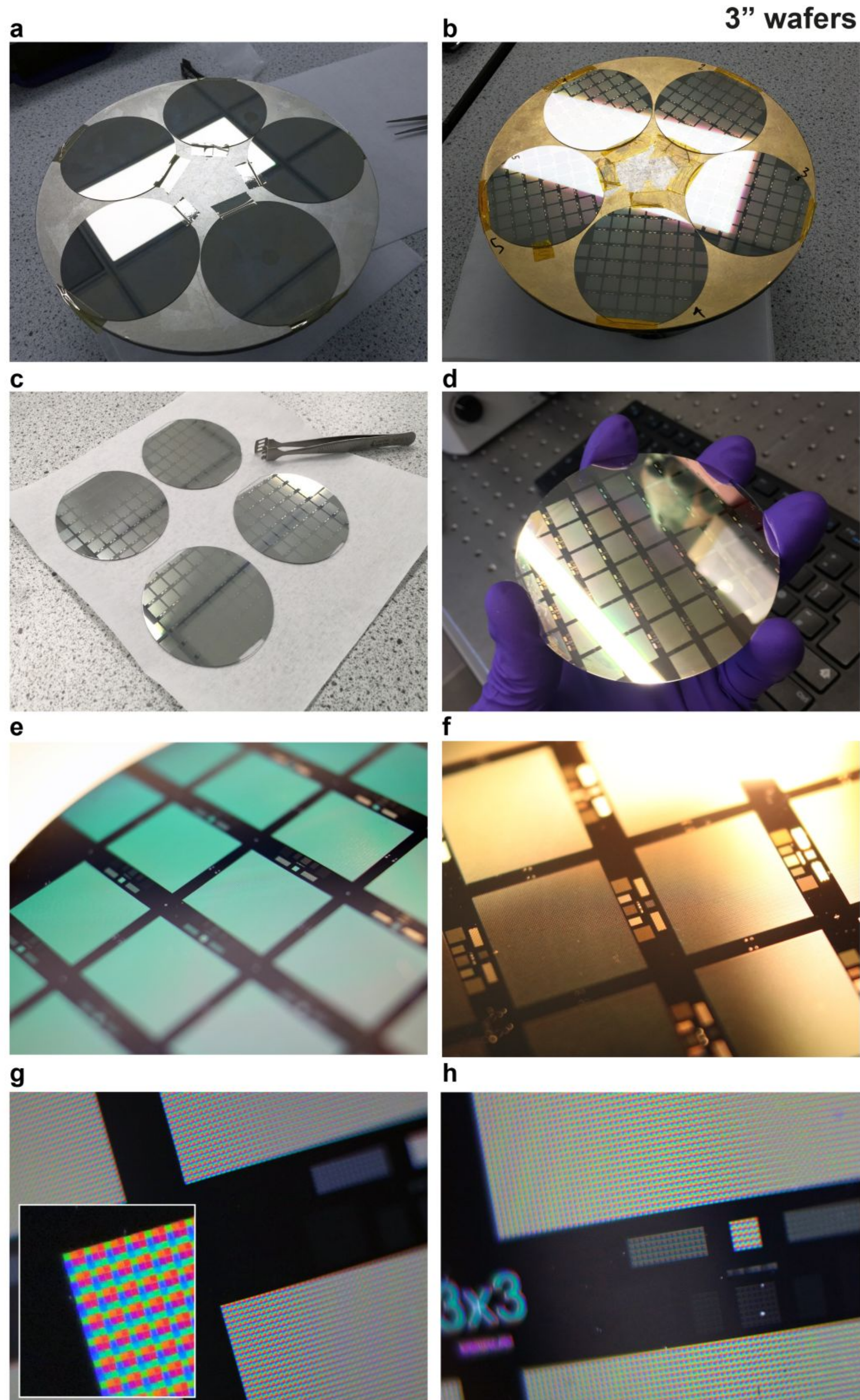

Supplementary Figure S20. Photographs of wafer-based MSFAs.
(a) Five 3”wafers post-first mirror deposition and pre-insulator (resist) grayscale lithography step. (b) The same wafers, after grayscale lithography step, post-second mirror deposition; i.e. finished wafers. The wafers in both images are attached to the e-beam evaporator wafer chuck. (c ,d) Finished wafers removed and ready to optically characterize. A macro lens with DSLR camera is used to image a wafer in both transmission (e) and in reflection (f), with LED backlight and halogen bulb light respectively. Due to the relatively large pixel size (30 microns), an increase in magnification reveals the MSFA mosaic details; (g) and (h) show different regions of a MSFA wafer in transmission with clear identification of the mosaic (repeating unit cell).

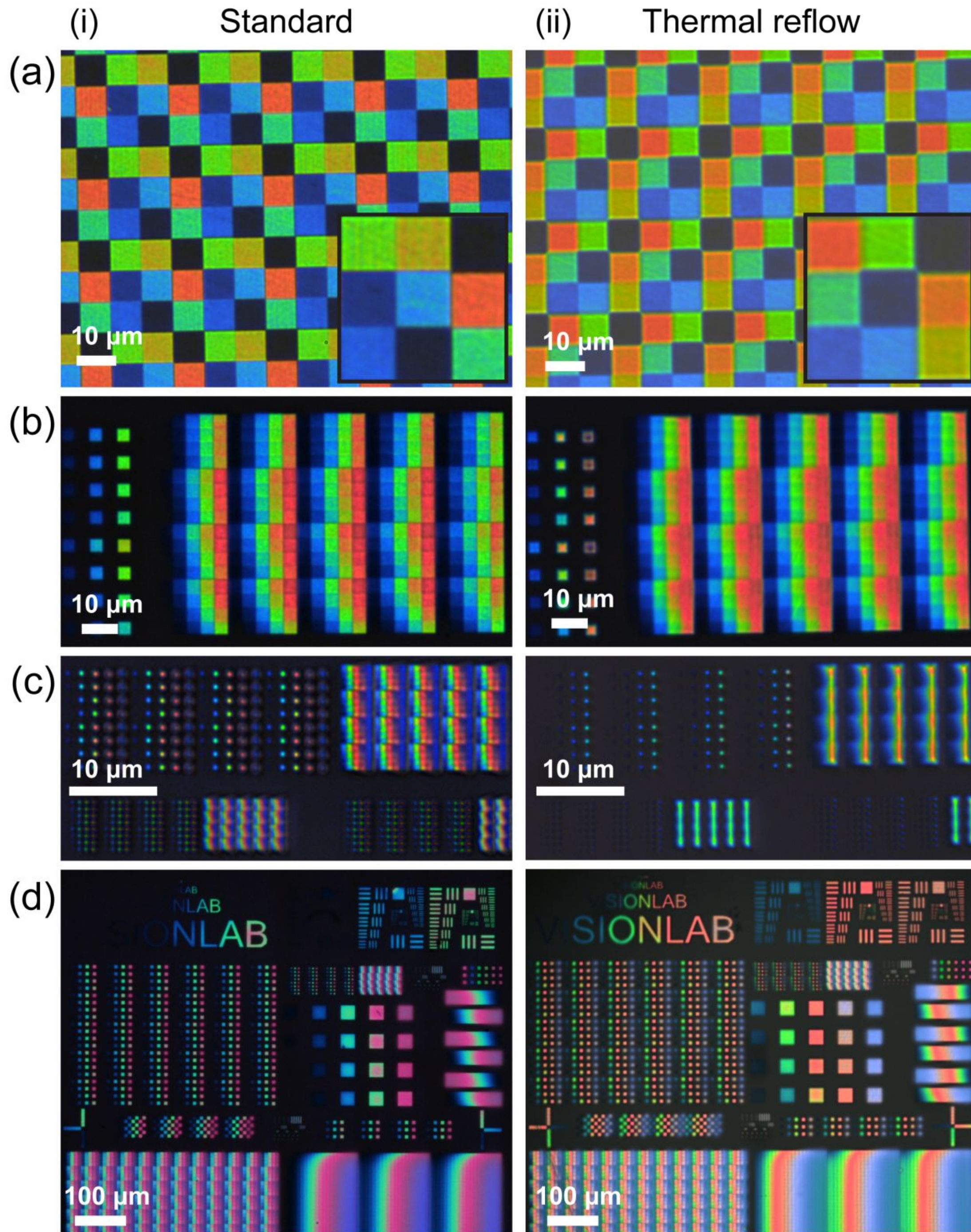

Supplementary Figure S21. Resist reflow visualized. Conditions: 100ºC for 30s; with samples (a) 8.8 µm pitch pixel MSFA, (b) 3.75 µm pixel pitch pixels and (c) 900 nm (upper rows) and 460 nm (bottom rows) pixels. (d) Conditions: Pre-resist development thermal reflow, using 100ºC for 1min; with custom resolution dose test. This is an example of a treatment to lower the dose applied to sample, as the temperature treatment here makes the resist harder to develop, and thus thicker.

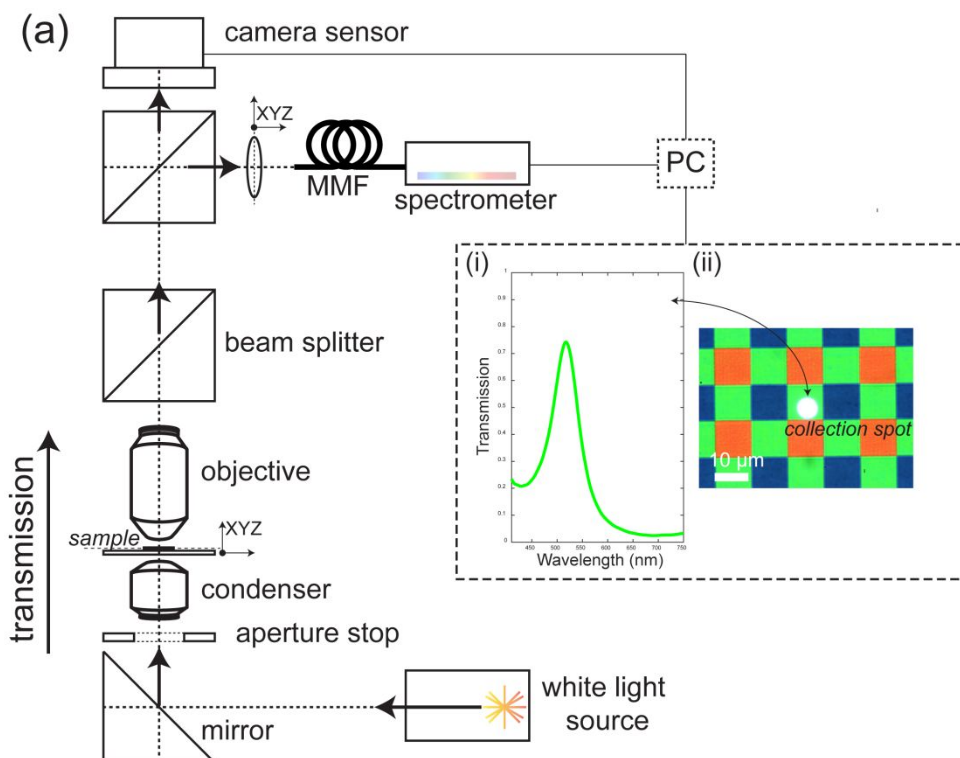

Supplementary Figure S22. Optical characterization schematic. The MSFAs are optically characterized using a modified Olympus BX-51 microscope: System schematic in (a). A 100W halogen lightbulb (V100WHAL-L; Philips 5761) illuminates the samples through a condenser (total light controlled via an aperture stop). A range of Olympus objectives (5—100x) are used for imaging the sample surfaces. Transmission is normalized through a glass cover slip (which the samples rest upon) and a 525 µm thick borosilicate glass (bright state). The two output paths are to a camera sensor and spectrometer to obtain magnified images of the sample and its corresponding transmission spectra respectively. (i) and (ii) show the information obtained from this arrangement: the transmission spectrum (i) and image of the sample surface in transmission (ii). The spectra are obtained using an Ocean Optics HR2000+ spectrometer and Ocean Optics Oceanview software

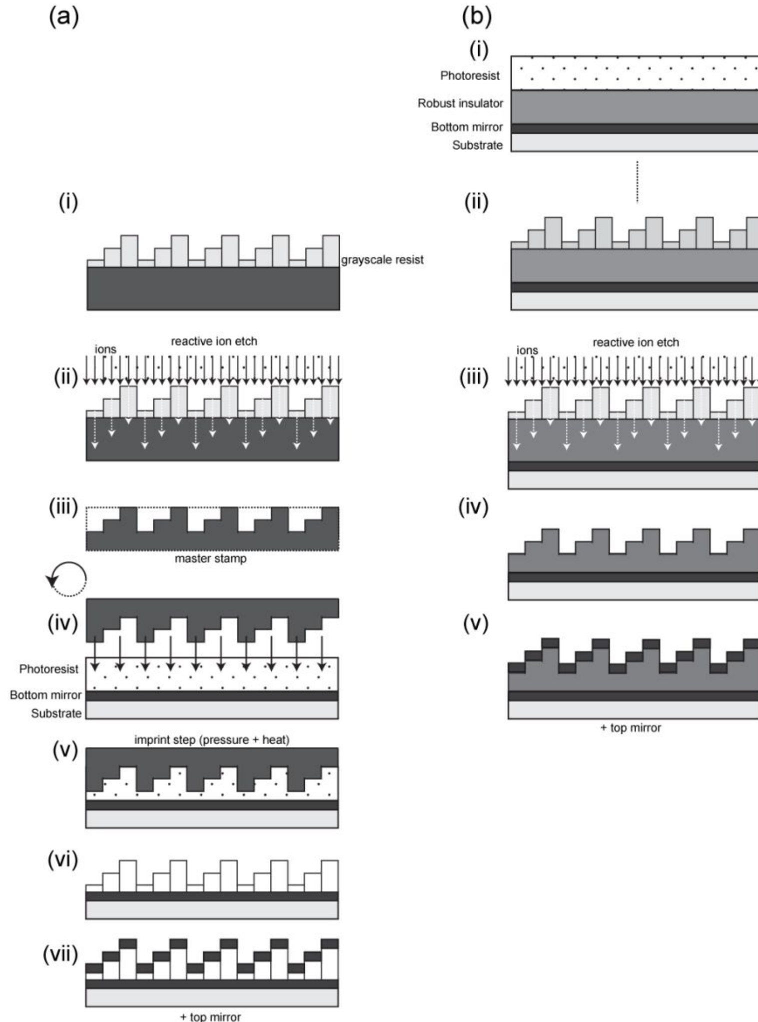

Supplementary Figure S23. Concept: Master stamp processing
(a) ***Grayscale master stamp.*** (i) Grayscale resist pattern atop of the master stamp material. This has been produced through any means (EBL / PL), it is not important which is used here. (ii) Etching step (RIE or otherwise): The resist and master stamp material is etched anisotropically, whereby etch thickness into the stamp material is determined through the resist thickness. If RIE is used, this step is performed using heavy ions bombarding the sample. RIE and imparting the pattern is a known process. (iii) The resultant master stamp is produced. (iv) Rotating the stamp and bringing into contact with a polymer (photoresist or otherwise) atop of a mirrored substrate. (v) Imprinting / moulding step: Stamping into the polymer, and incorporating a pressure + heat step (not exclusively necessary). (vi) Removing the master stamp leaving the imparted master stamp pattern into the polymer. (vii) The top mirror is deposited which creates a cavity (metal-insulator-metal geometry or otherwise) and spatially variant filters are subsequently produced.

(b) ***Robust insulator.*** (i) i. The starting material includes an insulator layer atop the bottom mirror, which is not the photoresist to be patterned. It has been deposited prior to the lithographic step. An example of a good material here is SiO2 (e.g. quartz). (ii) The lithographic step (EBL / PL) has been performed to produce a grayscale pattern into the photoresist. (iii) Etching step (RIE or otherwise): The resist and 'robust' insulator material is etched anisotropically, whereby etch thickness into the insulator is determined through the resist thickness. If RIE is used, this step is performed using heavy ions bombarding the sample. RIE and imparting the pattern is a known process. (iv) The final 'robust' insulator atop the bottom mirror layer and substrate, which has

taken the form of the grayscale resist thickness profile. (v) The top mirror is deposited which creates a cavity (metal-insulator-metal geometry or otherwise).

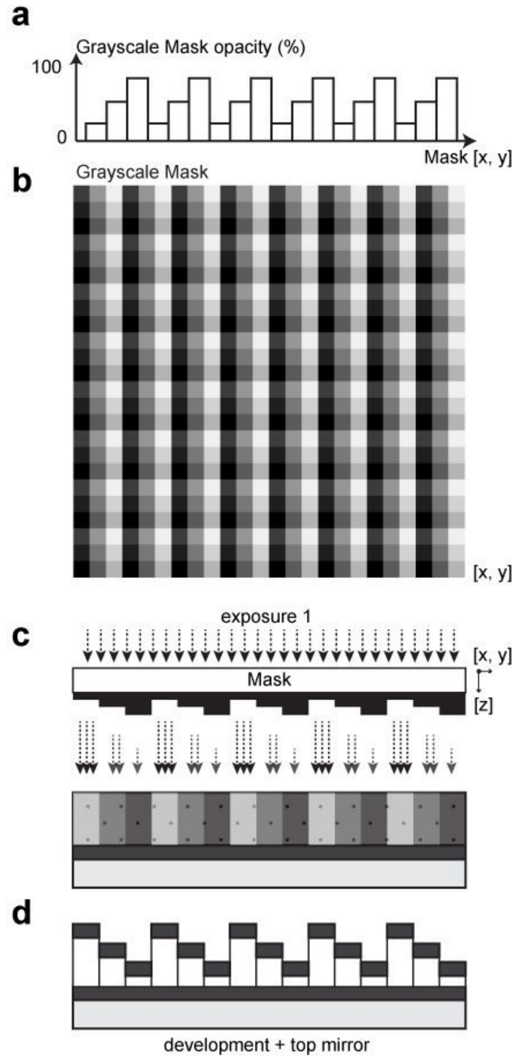

Supplementary Figure S24. Concept: MSFA manufacture using a grayscale Cr photomask (a) Grayscale mask opacity, with corresponding visual representation of the grayscale photomask (b) with 2D variation in levels of opacity. (c) Optical flood exposure, whereby Cr thickness governs transmittance, hence imparted exposure dose into the photoresist. (d) Resist development results in a 3D varying resist height (cavity), and through top mirror encapsulation provides spectral filtering across the device.

References

1. Lumerical Inc. www.lumerical.com/tcad-products/fdtd/.
2. Kajtár, G., Kafesaki, M., Economou, E. N. & Soukoulis, C. M. Theoretical model of homogeneous metal-insulator-metal perfect multi-band absorbers for the visible spectrum. *J. Phys. D. Appl. Phys.* **49**, 55104 (2016).
3. Li, Z., Butun, S. & Aydin, K. Large-area, Lithography-free super absorbers and color filters at visible frequencies using ultrathin metallic films. *ACS Photonics* **2**, 183–188 (2015).
4. Naik, G. V., Shalaev, V. M. & Boltasseva, A. Alternative plasmonic materials: Beyond gold and silver. *Adv. Mater.* **25**, 3264–3294 (2013).
5. McPeak, K. M. *et al.* Plasmonic films can easily be better: Rules and recipes. *ACS Photonics* **2**, 326–333 (2015).
6. Williams, C., Rughoobur, G., Flewitt, A. J. & Wilkinson, T. D. Single-step fabrication of thin-film linear variable bandpass filters based on metal–insulator–metal geometry. *Appl. Opt.* **55**, 9237 (2016).
7. Dodge, M. J. Refractive properties of magnesium fluoride. *Appl. Opt.* **23**, 1980 (1984).
8. Frey, L., Masarotto, L., Armand, M., Charles, M.-L. & Lartigue, O. Multispectral interference filter arrays with compensation of angular dependence or extended spectral range. *Opt. Express* **23**, 11799 (2015).
9. Skauli, T. *et al.* Compact camera for multispectral and conventional imaging based on patterned filters. *Appl. Opt.* **53**, C64 (2014).
10. Tseng, A. A., Chen, K. & Chen, C. D. Electron Beam Lithography in Nanoscale Fabrication : Recent Development. **26**, 141–149 (2003).
11. Takigawa, T., Kawabuchi, K., Yoshimi, M. & Kato, Y. High voltage electron beam lithography. *Microelectron. Eng.* **1**, 121–142 (1983).
12. Schleunitz, A. *et al.* Novel 3D micro- and nanofabrication method using thermally activated selective topography equilibration (TASTE) of polymers. *Nano Converg.* **1**, 7 (2014).
13. Macleod, H. *Thin-Film Optical Filters*. (Institute of Physics Publishing, 1986).